Vol. 43, No. 2 (2021) 200-210, DOI: 10.24874/ti.925.08.20.12

Tribology in Industry

www.tribology.rs

RESEARCH

Sliding and Corrosion Wear of Magnetron Sputtered TiO_2 Films Deposited with Different Argon and Oxygen Mixtures

W. Aperador[a,*], J. Bautista-Ruiz[b], J.C. Caicedo[c]

[a]*Universidad Militar Nueva Granada, carrera 11 101-80, Bogotá, Colombia,*
[b]*Universidad Francisco de Paula Santander, avenida Gran Colombia 12E-96, San José de Cúcuta, Colombia,*
[c]*Universidad del Valle, calle 13 100-00, Cali, Colombia.*

Keywords:

Titanium oxide
Corrosion
Tribology
Titanium
Surface modification

* Corresponding author:

Willian Aperador
E-mail: g.ing.materiales@gmail.com

Received: 28 August 2020
Revised: 12 October 2020
Accepted: 15 December 2020

A B S T R A C T

Were produced TiO_2 thin coatings prepared, on substrates pure Titanium using a deposition by magnetron sputtering technique, the percentage of oxygen was varied, to study the behavior in terms of friction coefficient corrosive fluids such as those related to the human body. Electrochemical Impedance Spectroscopy (EIS), wear tests with a tribometer, were performed to obtain the tribo-corrosion mechanism of deterioration, taking into account the dual corrosion wear system. The phases were identified by X-ray Photoelectron Spectroscopy (XPS) high resolution. It is determined through the tests performed that the surface treatment has a different effect for each percentage of oxygen influenced by the simulated body environments. The wear performance analysis indicated that the TiO_2 film's protection had increased as the percentage of oxygen in the gas mixture (Ar/O_2) varied and other synthesis parameters such as deposition time, target power, and substrate temperature remained constant.

1. INTRODUCTION

The Titanium dioxide TiO_2 has applications in electrochemical, photocatalysis, photoelectrochemistry, hydrogen production. Like gas sensors, corrosion protection, self-cleaning systems, solar cells, biomaterials, and other applications [1-3]. Because of the properties of ceramics, they can be used as electrical and transparent insulators. They can be modified with additives to make these materials appropriate for waveguides, modulators, and detectors. Nanocrystalline TiO_2 coatings are used in metal surface treatment to improve mechanical properties and applications such as insulation and anticorrosive barriers [4,5]. Thin films of TiO_2 deposited with physical vapor deposition exhibit adequate homogeneity, composition, and structure are controllable. The coatings low processing temperature, continuity on the surface, and the possibility of obtaining the anatase and rutile phase [6,7].

Between the methods of obtaining thin films exist the chemical and physical processes, the most employed being the so-called sputtering, an advantage of the technique are: high homogeneity of the coatings, high chemical and mechanical stability of the same, possibility of oversized coating substrates at a relatively low cost [8-11]. The steel AISI 316LVM undergoes pitting corrosion, which has lead to its replacement with other materials as titanium alloys [12-15]. It generates the inert character as it does not react against bone, tissue, or body fluids. Surface modification is required to create biocompatibility improve the finishing aspect, and increase the lengthy expected service life of medical devices such as needles, drills, and different components that wear out and are in various mechanisms used in biomedical and dental applications. These instruments have proven to offer better edge conservation so that coated surgical instrumentation remains sharp, reduced wear between the components to prevent corrosion [16,17].

The body fluids in contact with a surface generate biofilms as a cell growth required for osseointegration [18]. For that reason, the purpose of an implant is to integrate organic and inorganic materials. In that case, the inorganic material is TiO_2, and the cell metabolites needful a surface roughness, and so forth, tissues generate growth on the surface, forming biofilms [19,20]. They are thus inhomogeneously distributed on the surface area of coatings and also tend to be non-continuous. Such biofilms induce temporary changes in the so-called cathode and the anodic regions and can result in considerable damage to zones immediately around the metal and can influence corrosion phenomena, as is the situation concerning to 316LVM stainless steel [21].

The damaging effects of biofilms include reducing the mechanical properties and the deterioration of materials by pitting corrosion in many cases, problems with stress corrosion cracking [22]. The application of titanium oxide (TiO_2) coatings allows improving osseointegration, cytotoxicity, cell growth, and antibacterial properties.

The presented research is associated with wear and some other studies about corrosion. However, the synergy between wear and corrosion has not been reported [23,24].

This paper evaluated the variation of oxygen concentration in the production of TiO_2 thin films obtained by the magnetron sputtering method. The tests performed to determine their properties were wear, corrosion, and wear corrosion synergy, establishing that the percentage increment in mixture Ar/O_2 improved its response to wear. The aim is to verify that equitable combinations are the most acceptable to deterioration processes, resulting in appropriate stability to be used in the field of biomaterials.

2. MATERIALS AND METHODS

TiO_2 thin films produced on titanium grade 2 substrates using the magnetron sputtering technique (PVD). The magnetron equipment was operated in a direct current (DC) mode. The target of Ti of 10.16 cm diameter and 99.9% purity. The power (50 W), pressure (0.26 Pa), and temperature of the substrate (300°C), with variations in the percentage of oxygen (12.5, 25, 37.5 and 50 %) in the gas mixture (Ar/O_2). The specimens are processed using a solid cylindrical bar with a diameter of 1.908 cm. Several identical cuts are made along the longitudinal axis perpendicularly. The stakes are performed using an abrasive disc cutter and do not induce deformations and guarantee a clean-cut. Each piece is then assembled on a conventional lathe to obtain the required dimensions of the specimens and assure that their cross-sectional areas are parallel, i.e., by facing each of their faces to get a thickness of 0.5 cm.

The XPS experiments were carried in a SPECS Sage HR 100 spectrometer with a non-monochromatic X-ray source (Magnesium Kα), 1253.6 eV energy, and power applied 250 W. The equipment is calibrated using the $3d_{5/2}$ range of Ag with a full width at half maximum (FWHM) of 1.1 eV. The selected resolution for the spectra 15 eV of Pass Energy and 0.15 eV/step. All measurements were performed under an ultra-high vacuum (UHV) chamber at a pressure around $8x10^{-6}$ Pa. The samples have been assessing subsequently to the deposition with the technique PVD.

The coatings' wear was evaluated using a ball of linear sliding on a Reciprocal Plane of Motion. This technique allows simulating the characteristic movement of the prosthesis. A Nanovea, T2000 model tribometer was also used. The test

parameters are related to speed and load for a person who canine 1500 steps/day on average. A microscale machined bone pin, with a cylindrical shape, was used as a sliding pattern. The load applied in all tests was 15 N, the travel length was 888 m, and the sliding speed was 2 mm / s.

Electrochemical Impedance Spectroscopy (EIS) technique and an aerated physiological Ringer's solution at 37 °C was used to determine resistance values. The solution consisted of 9 g/l of NaCl, 0.4 g/l of $CaCl_2$, 0.17 g/l $CaCl_2$ and 2.1 g/l $NaHCO_3$. The study involved an electrical potential of 5 mV, and frequency ranges between 10 kHz and 0.001 Hz.

The interpretation of the experimental results in corrosion parameters requires the analogy between the coating with Ringer's physiological solution, through an electrical circuit and the adjustment with the Bode diagram. In the electrical circuit analogy, electric current flows through the different elements of the circuit. The result is a characteristic impedance (Z) and a phase angle response (φ). The identified regions are controlled by solution resistance (RΩ), double layer resistance, and bias resistance (Rp). Additionally, areas are dominated by capacitive elements.

In the coatings' tribochemical evaluation, the samples were subjected to corrosion conditions in a lubricant (Ringer's physiological solution). In the tests, an arrangement of three electrodes was available, the reference (Ag/AgCl), the counter electrode (platinum wire), and the working electrode (the sample to be analyzed). The area of analysis was 1 cm^2. A kit was used and using a Gamry potentiostat (Model No. PCI 4/750). The effect of corrosive wear, together with mechanical wear, was carried out under the same conditions described previously in the two techniques (electrochemical and tribological). The applied load was 15 N. The load value is related to the contact pressure of a person of average weight on a prosthesis. This study's objective was to analyze the type of wear produced when the implants contact fluid and the kind of movement that simulates the conditions according to the reciprocal pin-on-flat action.

3. RESULTS AND DISCUSSION

The Figure 1 observed that the cross-section thickness of the TiO_2 film uniform thin layer thickness of 0.91 ±0.07 μm. A columnar microstructure is evidenced with a preferential growth direction due to the rotation of the substrate.

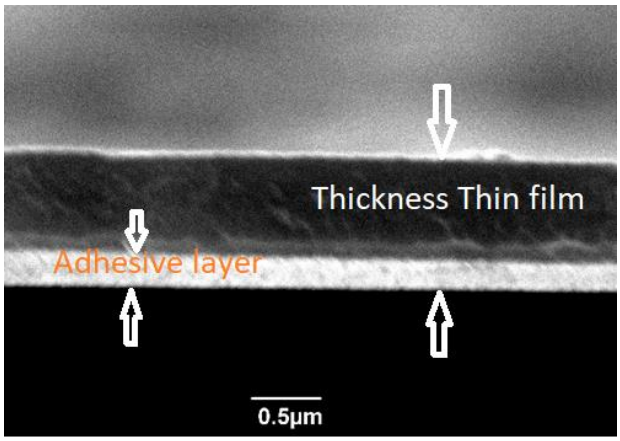

Fig. 1. SEM images of the cross-section of TiO_2.

The Figure 2 (a-d) shows the roughness of the variations of TiO_2. The Figure 2a illustrates that the 12.5 % film depicts a topography with regular texture, exhibiting certain grain homogeneity with similar dimensions. Not more than three or four crests on the surface can be observed. The surface roughness has been 91.5 ±0.1 nm. In Fig. 2b, the film establishing relations 25 % presents similar topography on the surface. It also explains some isolated crests few small cones sharp with an increase in the height profile, with an average roughness of 73.2 ±0.5 nm in the Fig. 4c corresponding to the ratio of 37.5 % shows the most prominent texture, the roughness of the material would have 56.7 ±0.3 nm. Lastly, in Fig. 2d displays a uniformly smooth texture for a 37.5 % ratio, self-evident in a decrease in roughness, 25.7 ±0.3 nm. Hence, the thick rutile TiO_2 layer for the oxidized sample will significantly promote the hydrophilic properties revealed with a reduction of static contact angle according to the literature [25].

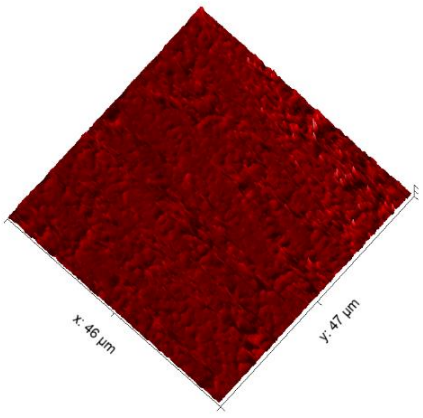

(a)

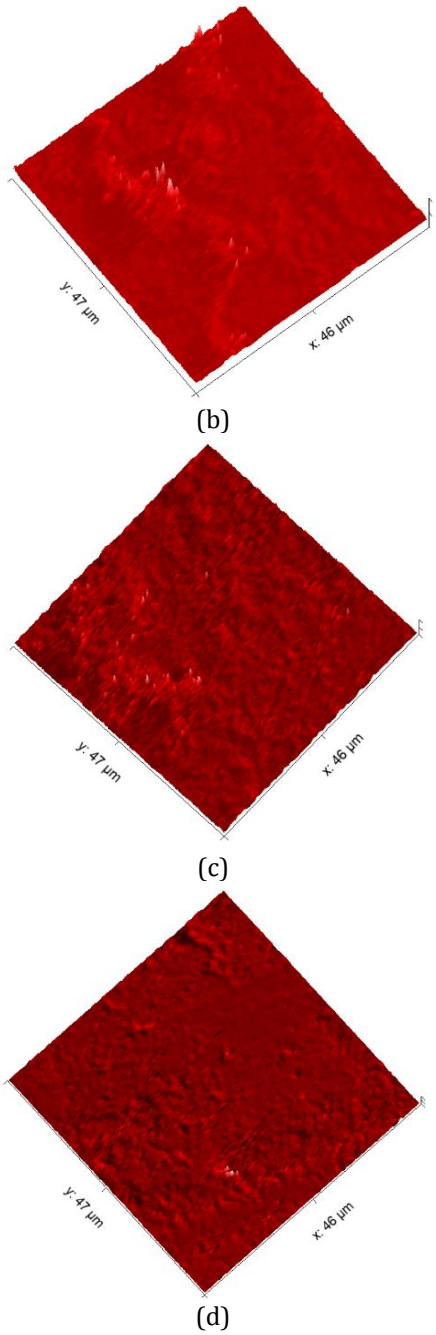

Fig. 2. AFM imagens of films of (a) TiO_2 12.5 %, (b) 25 % of Ar/O_2,(c) 37.5 % of Ar/O_2 and (d) 50 % of Ar/O_2.

The Figure 3 presents the results of the roughness. The surface coating was evaluated four times. The statistical treatment of the data allows determining parameters such as the average roughness (Ra).

As illustrated in Fig. 4, the high-resolution XPS spectra obtained for TiO_2 are presented. The Titanium ranges are evidenced to be shifting towards higher energy zones with increased oxygen content. Regarding the TiO_2 coating, with 12.5% Ar/O_2, only one peak presents in all spectrum. For 25% Ar/O_2, the Titanium doubling peaks are at the binding energies of 532.17 ±0.1 eV and 534.09 ±0.1 eV, both, respectively. This doublet position is similar to the reported one for Titanium and other Ti-O compounds. On the 37.5%Ar/O_2 coating, the doublet is displaced to 534.13 ±0.1 eV and 532.02 ±0.1 eV. With a layer containing 50%Ar/O_2, the pair is replaced even more toward lower bonding energy areas, at 533.79 ±0.1 eV and 531.65 ±0.1 eV. This position has been indexed for the TiO_2 compound. The principal peak is at the binding energy of 532 ±0.1 eV for the TiO_2 coating. Such energy is reported for both metallic Titanium and TiO compound. On the other hand, for the layers with a ratio of Ar/O_2, at different percentages, this peak demonstrates a significant displacement to higher binding energy, located at 534 ±0.1 eV, with a relationship to TiO_2. These results are corroborated with the research of Wang et al. [26].

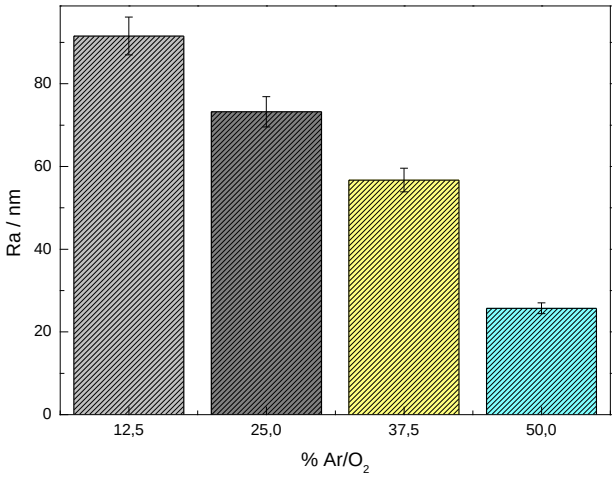

Fig 3. Average roughness graph as a function of the percentage of different argon and oxygen mixtures.

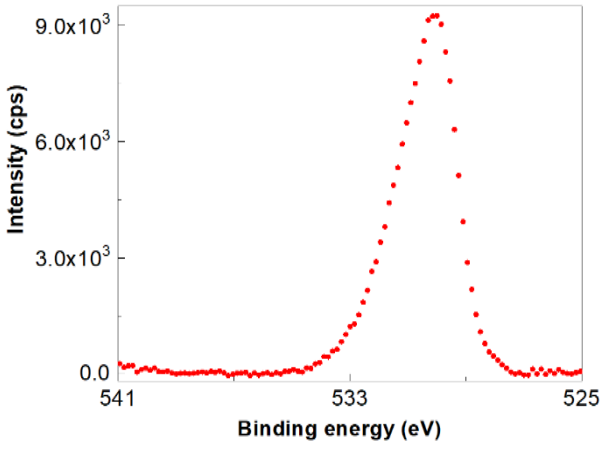

(a)

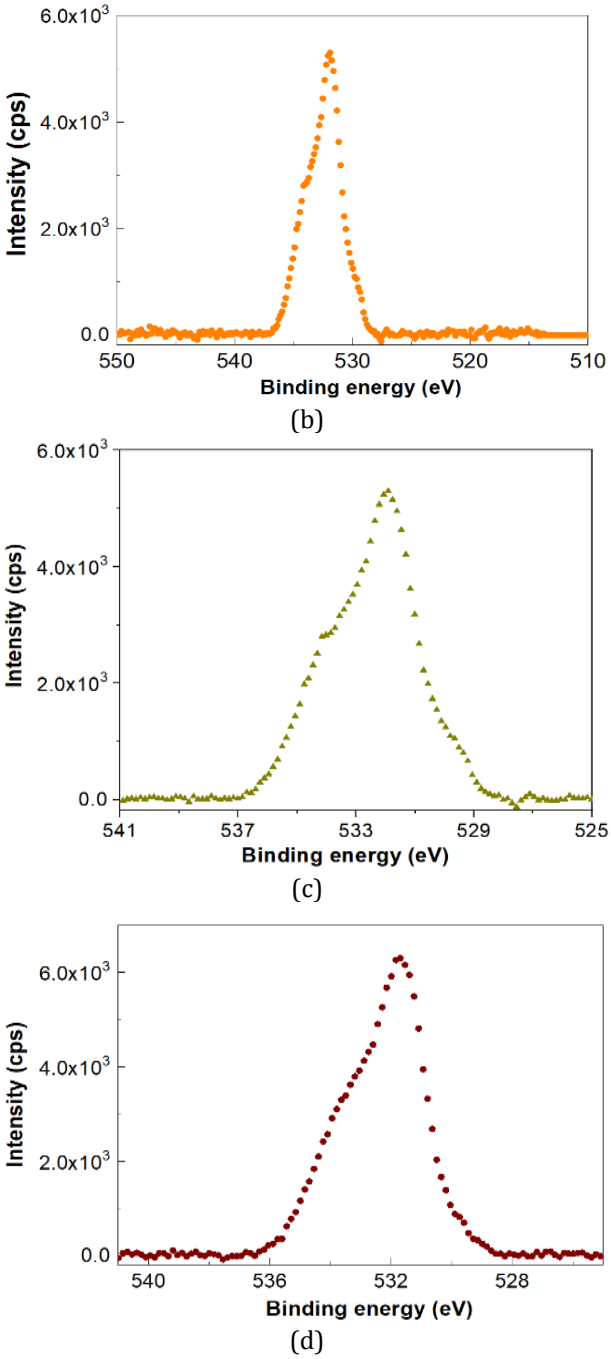

Fig. 4. (a) XPS results for the TiO_2 peak, with a ratio of 12.5 % of Ar/O_2. (b) two peaks at 532.17 ±0.1 eV and 534.09 ±0.1 eV are attributed to the Ti-O-Ti bonds, related with a rate of 25 % of Ar/O_2.(c) two peaks at 534.13 ±0.1 eV and 532.02 ±0.1 eV, assigned to relation 37.5 % of Ar/O_2 and (d) two picks at 533.79 ±0.1 eV and 531.65 ±0.1 eV associate itself a ratio 50 % of Ar/O_2.

Coefficients of friction (COF) are indicated (Fig. 5); for the essays, without Ringer's physiological solution, an initial increase was obtained, afterward, as the test increasingly stabilized with relation to values of the average coefficient of friction. These can be appreciated in Fig. 4, where the graphic of the coefficient of friction versus distance is available. The tribology tests have been developed with potential implementation as the knee prosthesis, specifically designed to resist mechanical stress and excessive exercise in the joint daily. They should consider a distance of 800 m, which is fatigue, because of the average load applied daily in inpatient recovery conditions.

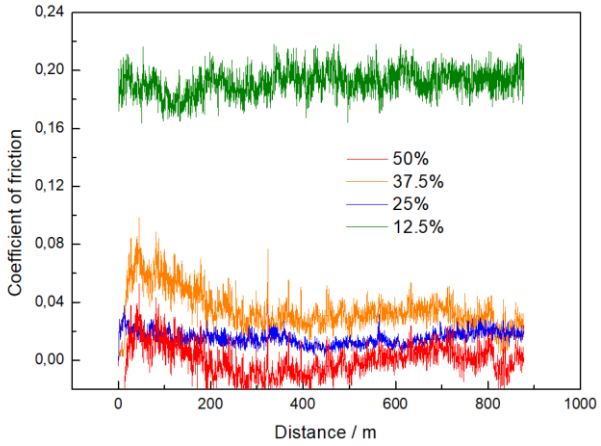

Fig. 5. The relationship between the friction and distance coefficient for the TiO_2 under a load of 15 N dry without Ringer's solution.

After 200 meters, the COF value is approximately in a stability zone, although the reference is taken to determine an average was 800 meters. It should, therefore, be the observed value of 0.2 for a percentage of 12.5%Ar/O_2, a very high value and one that differs from other values reported in high rates (25 to 50 % Ar/O_2) by approximately being five orders of magnitude more than of the coefficient of friction under 0.1 for 50 % ratio of Ar/O_2. An increase and decrease in the values of the coefficient of friction are also identified. In the so-called dry tests, because with the rise in the test time, the temperature increases, and the appearance of oxides on the surfaces produces an increment of hardness (The oxide layer is the result of the accumulation of oxide debris and oxidized metallic particles). Therefore, it decreases the friction coefficient, making it a suitable system for prosthetic-type coatings. However, some unwanted porosities may occur due to the increased roughness parameters. Nevertheless, some grains begin to appear as particle limits, but a smooth surface can still be detected in all coatings and large grains in the material's microstructure.

In Figure 6 shows the performance of the dual wear and corrosion system together. The same conditions as the system without the use of

lubrication have been evaluated. It has now been determined that the friction coefficient is reduced for the four scenarios compared to figure 4. In all assessed systems are two areas where different values of friction are reported. The first area represents a progressive increase in friction following the tensile force applied to the interface. This period extends up to 20 meters, and after this, the first amounts of friction modified are introduced gradually. A transition area is observed - region 2 - characterized by a stabilization in the coefficient of friction. Such behavior is assigned to the effect of the fluid because surface roughness comes under the medium category. There is no effect due to the low sliding velocities. The generation of the initial layers of oxide is a delay in the formation and later are consumed rapidly, not high temperatures are produced (due to the controlled 37 °C). Additionally, there is predominant wear by adhesion.

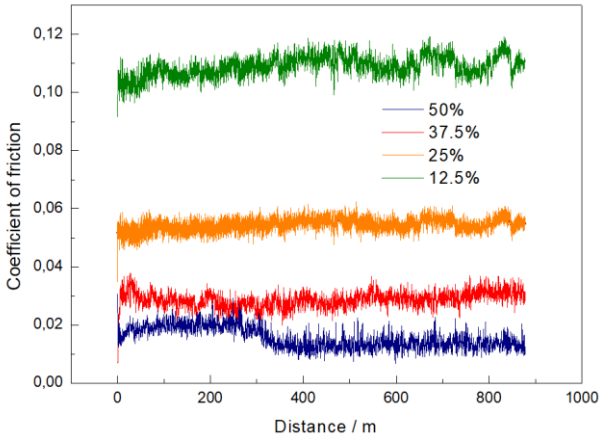

Fig. 5. Simultaneous corrosion-friction-wear phenomena resistance of coatings of the TiO_2 thin films obtained under a load of 15 N.

Similarly, in Fig. 5, each coating coefficient's value shows a similar relationship to the previously analyzed case. In other words, the ratio is inversely proportional to the increase of the Ar/O_2 ratio, and the value of the coefficient decreases. Almost to shallow values in which it is possible to indicate that the deterioration is negligible or very nearly zero, for the 50%Ar/O_2 ratio, that is due to the formation of a slightly oxidized layer adequate lubrication. Similar results also have been reported by other researchers [27].

The Figure 6 represents the coatings and the variation of impedance and phase angle as a function of frequency for systems assessed only for the effect of degradation in the simulated fluid. At different frequencies, two slope changes are evident, which correspond to the resistor-capacitor circuits' time constants. The most significant % Ar/O_2 value in the system corresponds to the maximum phase angle. This value is typical of capacitive elements, whereas coatings with lower % Ar/O_2 values have lower phase angles. This explains the electrolyte-coating interface's less efficient operation caused by the layer's corrosive effect (Table 1). It is possible to observe the change in the phase angle curves' slope concerning the frequency logarithm. For the coating with 12.5 % of Ar/O_2, such a layer displayed the lowest phase angle value, demonstrating the damage in the film. The remaining coatings in percentages ranging from 25 to 50 %, showed changes in slope related to the occurrence of several electrochemical processes. However, although these three systems show a gradient variation, there were less capacitive phase angles, explained by the coating-metal interface. The best system in the adhesive response is 50%Ar/O_2 (Table 1) since this coating does not have an inflection shift as it is observed in the other materials.

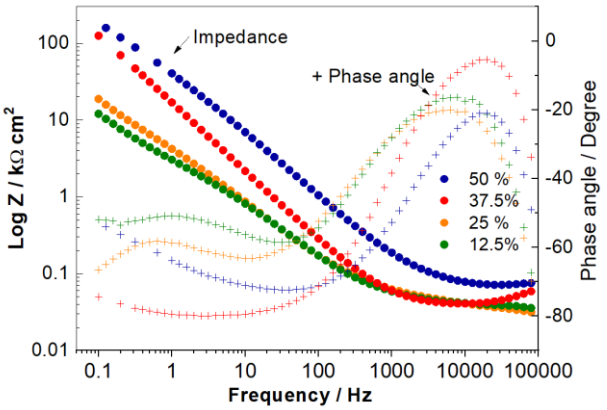

Fig. 6. Bode plot of the coated TiO_2 with different ratio Ar/O_2, in Hanks solution.

Nevertheless, the phase angle values were lower due to the coating's deterioration by the effect of corrosion on the surface. Following the variation in the coating-titanium interface slope, the phase angle values appear to be less capacitive for the two cases with a smaller percentage of 12.5 and 25 %, demonstrating the damage generated by wear was superficial and did not reach the coating-to-metal interface. In the low frequencies, for the systems, 37.5 and 50 %, a decrease in the phase angle to resistive values are presented, related to the coating's load transfer

resistance. The phase angle versus frequency curves of TiO_2 coatings describes the performance in an active layer due to the curve's considerable convexity. Since the contact with the fluid, the coating remains active and does not get altered by the contact with the chlorine ions present in the Ringer's physiological solution.

Table 1. Parameters used in the simulation of impedance data in Ringer's solution.

Parameters	Ar/O_2			
	12.50	25	37.50	50
R_Ω (Ω cm^2)	0.030	0.038	0.062	0.078
Y_{P1} (F cm^{-2} s$^{-(1-\alpha_1)}$) $\times10^{-9}$	1.01	1.89	2.19	72.82
α_1	0.88	0.90	0.96	0.97
R_1 (kΩ cm^2)	0.0066	0.074	0.090	0.311
Y_{P2} (F cm^{-2} s$^{-(1-\alpha_2)}$) $\times10^{-5}$	2.19	9.80	493	113
α_2	0.79	0.82	0.89	0.84
R_2 (kΩ cm^2)	12.52	18.95	129	202

The coating-metal interface is represented in Fig. 7. For four mechanisms: dual corrosion-wear system, variation in the intensity of the peaks, and the time constants show from the load applied during the test, the capacitors charging time is affected by the values at high frequencies in systems ratio 50 to 25% Ar/O_2. However, system 12.5 % generates that the capacitor's charge decreases the dielectric character of the TiO_2 film, to the other evaluated systems. The concavities in the phase angle versus frequency plot show that the titanium oxide layer on the Titanium behaved in all cases as a compact coating. The low deterioration of the capacitive character is attributed to the surface damage by corrosion-assisted sliding wear effects; the low frequencies of the impedance exhibit similar properties for all three coating test conditions. Since as the frequency decreases, the impedance increases, these values are identical the better the Ar/O_2 ratio, the comparison of the time constant at low frequencies, for the two systems 50 and 37.5 %, results in a higher time constant, which is equivalent to increased load transfer resistance and more stability. The deterioration processes explain the behavior of coatings at low frequencies at the metal-coating interface after the wear test with a load of 15 N. From the study, can be concluded that the coatings showed a lower reduction due to the effect of loss of mass concerning the system evaluated for corrosion only (Table 2). The deterioration conditions are lower with the dual system. This trend indicates decreased resistance to charge transfer and corrosion-wear damage generated by the oxide film formation kinetics at 37 °C. The oxide is adherent to the coating and determines a passive surface under the coating moderately inert condition. When comparing the COF results of Fig. 5, it was determined that the surfaces (ridges and valleys) have low levels between them. This behavior is typical of a linear kinematics situation. Other researchers [28] have also made a similar conclusion.

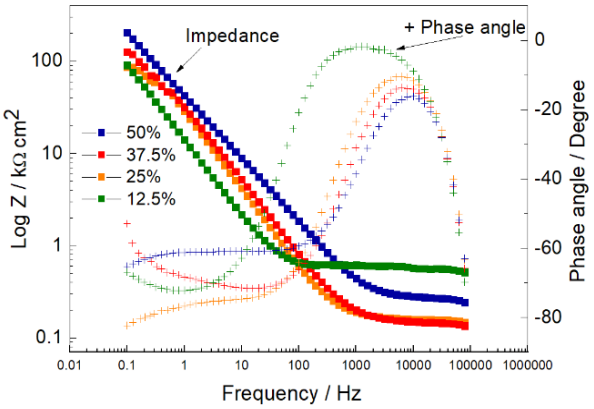

Fig. 7. Bode plot was used to describe the corrosion and wear characteristics of TiO_2.

Table 2. Electrochemical impedance parameters on TiO_2.

Parameters	Ar/O_2			
	12.50	25	37.50	50
R_Ω (Ω cm^2)	0.54	0.15	0.13	0.23
Y_{P1} (F cm^{-2} s$^{-(1-\alpha_1)}$) $\times10^{-10}$	9.83	3.56	4.58	4.84
α_1	0.78	0.85	0.86	0.93
R_1 (kΩ cm^2)	0.63	0.15	0.36	0.72
Y_{P2} (F cm^{-2} s$^{-(1-\alpha_2)}$) $\times10^{-4}$	6.19	4.09	29.11	71.42
α_2	0.65	0.74	0.89	0.93
R_2 (kΩ cm^2)	81.47	92.44	126.2	216.3

In that only case, the effect of corrosion is analyzed. The equivalent circuit for the four coatings evaluated is illustrated through two-time constants in the impedance curve Vs. Frequency, as presented in Fig. 8. The first corresponds to high frequencies parallel to the charge transfer resistance in the solution coated interface.

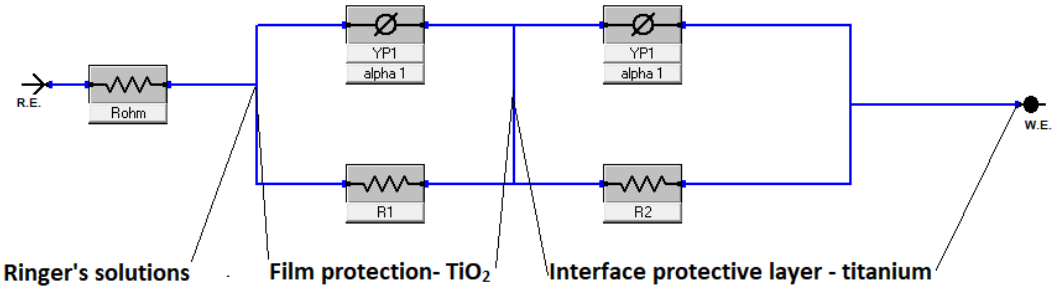

Fig. 8. Equivalent circuit.

The combination of these two processes is controlled by the charge transfer, adjacent to the coating's dielectric character. This process is the transfer of mass by ions from the solution and resorption ions of the layer. Finally, there is the time constant that represents the TiO_2 - titanium interface. For the case of the dual corrosion - sliding wear system, the same mechanism is obtained. The Bode diagrams are adjusted with an identical electrical model. The one-time constant associated with the deterioration in the coatings dielectric properties due to the 15 N load effect was applied during the sliding wear test.

Comparing the two systems against the one that has only contact with the Ringer's physiological solution is obtained the displacement towards higher frequencies and a significant peak of the phase angle curve of the coatings submitted to the tribological test compared to the one proposed to corrosion under static conditions, indicates the re-passivation of the system, in the surface of the coated material. In the Bode diagram, Fig. 7, it is possible to observe the impedance behavior at low frequencies for the four coatings submitted to corrosion-assisted wear. This trend reveals that a capacitive performance is produced for mixtures, which establishes an inhibiting factor directly proportional to the Ar/O_2 ratio.

In Fig. 9, the mechanism of wear evident from the bone's contact and the coatings, assisted by the fluid, is observed due to the demonstration of a decrease in wear rate employing the corrosion assessment tests. In each case, the related wear is from adhesive wear is supported by the secondary coatings cracking, similar to the literature [27]. Furthermore, the fluid may transport some of the broken material and transfer it in different coating regions because areas of loosened material are visible, as is the case of the system identified as 12.5 % (Fig. 9a).

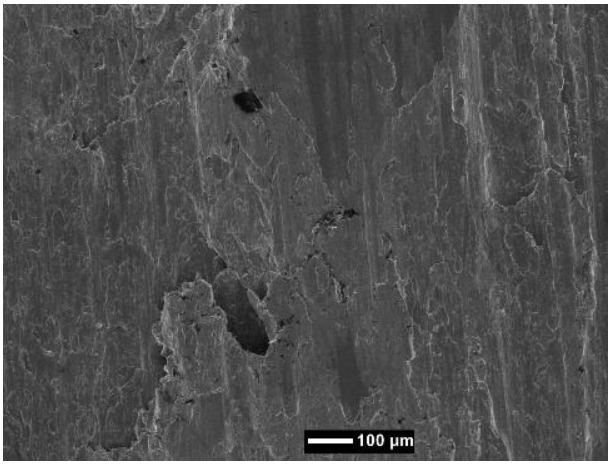

(a)

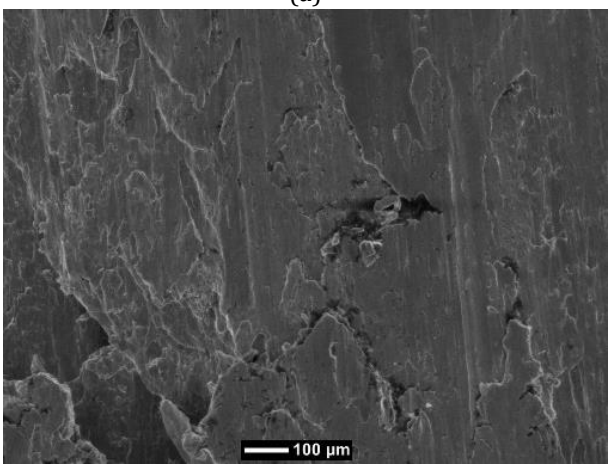

(b)

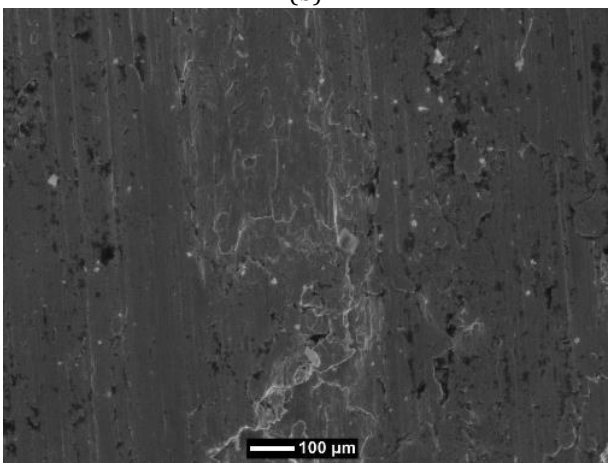

(c)

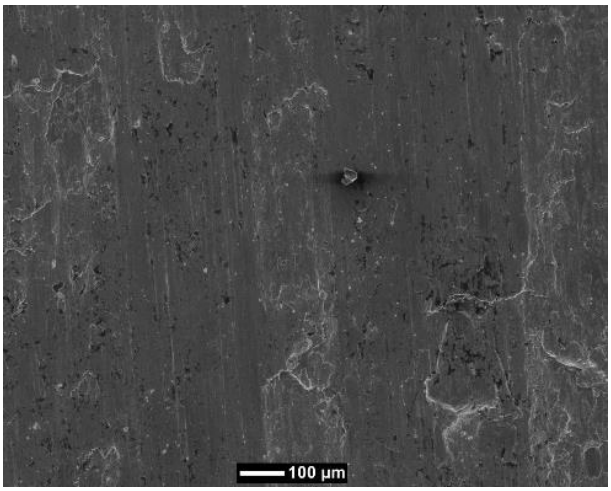

(d)

Fig 9. Micrographs where the type of wear generated on the coatings is determined, a) corresponding to 12.5 %, b) 25 %, C) 37.5 %, and d) 50 %.

In the micrograph of Fig. 9b, which corresponds to the 25 % ratio, detached particles can be identified, and it is possible to determine which particles are free of wear. In both cases, the friction value coefficient is the highest, with the other coatings analyzed. In the case of layers, with percentages of 37.5 and 50 %, the same wear mechanism was determined. However, the wear trace after testing is very smooth. This is due to the adhesion forces between the contacting surfaces, which generate cracks in the coating surface. The COFs are lower, indicating a slight deterioration of the films.

4. CONCLUSIONS

Thin films of titanium dioxide were grown using the magnetron sputtering technique. A necessary condition is to improve the crystallinity of the films and the deterioration properties according to the argon/oxygen ratio.

The variation of the oxygen concentration in the titanium oxide films has now been obtained. It was possible to establish that equal mixtures are that over there has the best response to degradation phenomena, generating adequate stability to be used in biomaterials.

The trend of polarization resistance (Rp) is a relationship of increasing O_2 concentration in TiO_2 films. With the lowest percentage corresponding to 12.5 %, the resistance to be polarized is low and increases as this oxygen ratio increases. Therefore, the system deposited with 50 % exhibits the best electrochemical and tribological behavior. This trend comportment can be associated with a more significant percentage of energy absorption bands of the active modes related to the TiO_2 bonds, as confirmed by the high-resolution XPS spectra analysis.

In tribological tests without fluid presence, the friction coefficient amounts to about 0.2, a low value compared to systems such as Titanium and its alloys.

The evaluation by EIS of the materials by modifying the Ar/O2 ratios allowed to establish that the phase angle is maximum for high Ar/O2 and the coatings are more efficient from the anticorrosive point of view. Compared with lower percentages in the Ar/O2 ratio, they allowed establishing smaller phase angles produced by the corrosive effect on the coating, leading to low anti-corrosion efficiency. To the layers supporting a load of 15 N, the impedance values were lower than those registered for the films exposed only to corrosion conditions due to the material's porosity and related with the wear curves and its good behavior against mechanical resistance.

Acknowledgement

This research was supported by “Vicerectoria de investigaciones Universidad Militar Nueva Granada” under contract ING 3123 validity 2020-2021.

REFERENCES

[1] J. Yu, J. Lei, L. Wang, J. Zhang, Y. Liu, *TiO_2 inverse opal photonic crystals: Synthesis, modification, and applications - A review,* Journal of Alloys and Compounds, vol. 769, pp. 740-757, 2018, doi: 10.1016/j.jallcom.2018.07.357

[2] M.M. Morsi, F.H. Margha, R.Morsi, *Effect of sintering temperature on the developed crystalline phases, optical and electrical properties of 5ZnO-2TiO_2- 3P_2O_5 glass*, Journal of Alloys and Compounds, vol. 769, pp. 758-765, 2018, doi: 10.1016/j.jallcom.2018.08.045

[3] M. Curti, G. López-Robledo, P. dos Santos Claro, J.H. Ubogui, C.B. Mendive, *Characterization of titania inverse opals prepared by two distinct infiltration approaches,* Materials Research Bulletin, vol. 101, pp. 12-19, 2018, doi: 10.1016/j.materresbull.2017.12.035

[4] W. Aperador, L. Yate, M.J. Pinzón, J.C. Caicedo, *Optical and semiconductive properties of binary and ternary thin films from the Nb-Ti-O system*, Results in Physics, vol. 9, pp. 328-336, 2018, doi: 10.1016/j.rinp.2018.02.060

[5] S. All, G. El-Shobaky, *Structural and electrical properties of γ-irradiated TiO2/Al2O3 composite prepared by sol–gel method*, Journal of Alloys and Compounds, vol. 479, iss. 1–2, pp. 91-96, 2009, doi: 10.1016/j.jallcom.2009.01.071

[6] M.K. Hossain, M.T. Rahman, M.K. Basher, M.J. Afzal, M.S. Bashar, *Impact of ionizing radiation doses on nanocrystalline TiO2 layer in DSSC's photoanode film,* Results in Physics, vol. 11, pp. 1172-1181, 2018, doi: 10.1016/j.rinp.2018.10.006

[7] Y. Ye, S. Kure-Chu, Z. Sun, T. Matsubara, G. Tang, T. Hihara, M. Okido, H. Yashiro, *Self-lubricated nanoporous TiO_2-TiN films fabricated on nanocrystalline layer of Titanium with enhanced tribological properties*, Surface and Coatings Technology, vol. 351, pp. 162-170, 2018, doi: 10.1016/j.surfcoat.2018.07.089

[8] S. Varnagiris, D. Girdzevicius, M. Urbonavicius, D. Milcius, *Incorporation of SiO_2 and TiO_2 additives into expanded polystyrene foam using physical vapor deposition technique*, Energy Procedia, vol. 128, pp. 525-532, 2017, doi: 10.1016/j.egypro.2017.09.073

[9] S. Shakir, H.M. Abd-ur-Rehman, K. Yunus, M. Iwamoto, V. Periasamy, *Fabrication of un-doped and magnesium doped TiO_2 films by aerosol assisted chemical vapor deposition for dye sensitized solar cells*, Journal of Alloys and Compounds, vol. 737, pp. 740-747, 2018, doi: 10.1016/j.jallcom.2017.12.165

[10] D. Li, A. Goullet, M. Carette, A. Granier, J.P. Landesman, *Effect of growth interruptions on TiO_2 films deposited by plasma enhanced chemical vapour deposition,* Materials Chemistry and Physics, vol. 182, pp. 409-417, 2016, doi: 10.1016/j.matchemphys.2016.07.049

[11] A. Shahryari, S. Omanovic, J.A. Szpunar, *Electrochemical formation of highly pitting resistant passive films on a biomedical grade 316LVM stainless steel surface,* Materials Science and Engineering: C, vol. 28, iss. 1, pp. 94-106, 2008, doi: 10.1016/j.msec.2007.09.002

[12] D.A. Florea, D. Albuleț, A.M. Grumezescu, E. Andronescu, *A step forward to overcome the current challenges in orthopedic industry and to obtain an improved osseointegration and antimicrobial properties,* Materials Chemistry and Physics, vol. 243, pp. 122579, 2020, doi: 10.1016/j.matchemphys.2019.122579

[13] Z. Xu, L. Yate, Y. Qiu, W. Aperador, E. Coy, B. Jiang, S. Moya, G.Wang, H. Pan, *Potential of niobium-based thin films as a protective and osteogenic coating for dental implants: The role of the nonmetal elements,* Materials Science and Engineering: C, vol. 96, pp. 166-175, 2019, doi: 10.1016/j.msec.2018.10.091

[14] P. Canepa, G. Firpo, R. Mattera, M. Canepa, O. Cavalleri, *Calcium and phosphorous enrichment of porous niobium and titanium oxides for biomaterial applications,* Surface and Coatings Technology, vol. 389, p. 125634, 2020, doi: 10.1016/j.surfcoat.2020.125634

[15] A. Çelik, M.T. Acar, T. Yetim, H. Kovac, A.F. Yetim, *Improving structural, tribological and electrochemical properties of Ti6Al4V alloy with B-doped TiO_2 thin films,* Tribology International, vol. 146, pp. 106210, 2020, doi: 10.1016/j.triboint.2020.106210

[16] T. Bai, Y. Fang, J. Wang, *Preparation and tribological properties of graphene/TiO_2 ceramic films, Ceramics International,* Ceramics International, vol. 43, iss. 16, pp. 13299-13307, 2017, doi: 10.1016/j.ceramint.2017.07.028

[17] J. Bautista-Ruiz, C. Ortiz, B. Parada, *Formation of thin sol-gel films for anticorrosive applications*, Tunja: UPTC, Colombia, 2008. (in Spanish)

[18] S. Jyothi, Y.V. Subba Rao P.S. Samuel Ratnakumar, *Natural product as corrosion inhibitors in various corrosive media: a review,* Rasayan Journal of Chemistry, vol. 12, no. 2, pp. 537-544, 2019, doi: 10.31788/RJC.2019.1225000

[19] M. Azadeh, S. Parvizy, A. Afshar, *Corrosion resistance and photocatalytic activity evaluation of electrophoretically deposited TiO_2-rGO nanocomposite on 316L stainless steel substrate,* Ceramics International, vol. 45, iss. 11, pp. 13747-13760, 2019, doi: 10.1016/j.ceramint.2019.04.071

[20] N.N. Zurita-Mendez, G. Carbajal-De la Torre, M. Estevez, *Evaluation of the electrochemical behavior of TiO_2/Al_2O_3/PCL composite coatings in Hank's solution,* Materials Chemistry and Physics, vol. 235, p. 121773, 2019, doi: 10.1016/j.matchemphys.2019.121773

[21] Y.H. Chen, W.S. Chuang, J.C. Huang, X. Wang, H.S. Chou, Y.J. Lai, P.H. Lin, *On the bio-corrosion and biocompatibility of TiTaNb medium entropy alloy films,* Applied Surface Science, vol. 508, p. 145307, 2020, doi: 10.1016/j.apsusc.2020.145307

[22] S. Agiladevi, S. Rajendran, *Electrochemical studies on the corrosion behaviour of metals and alloys in simulated Ringer's solution,* Rasayan Journal of Chemistry, vol. 12, no. 1, 22-31, 2019, doi: 10.31788/RJC.2019.1215037

[23] J. Bautista-Ruiz, W. Aperador, J.J. Olaya, *Effect of centrifugal speed on the anticorrosive properties of bismuth-silicon coatings by sol-gel on 316l substrates,* Rasayan Journal of Chemistry, vol. 11, no. 2, pp. 597-607, 2018, doi: 10.31788/RJC.2018.1122075

[24] J. Bautista-Ruiz, W. Aperador C. España, *Abrasive and Corrosive Wear of TiN / TiAlN and TiN / AlTiN Coatings*, Madrid: Eae-publishing, 2011. (in Spanish)

[25] C. Huh, S.G. Mason, *Effects of surface roughness on wetting (theoretical),* Journal of Colloid and Interface Science, vol. 60, iss. 1, pp. 11-38, 1977, doi: 10.1016/0021-9797(77)90251-X

[26] S. Wang, Y. Liu, C. Zhang, Z. Liao, W. Liu, *The improvement of wettability, biotribological behavior and corrosion resistance of titanium alloy pretreated by thermal oxidation,* Tribology International, vol. 79, pp. 174-182, 2014, doi: 10.1016/j.triboint.2014.06.008

[27] D. Xiong, Y. Yang, Y. Deng, *Bio-tribological properties of UHMWPE against surface modified titanium alloy*, Surface and Coatings Technology, vol. 228 pp. S442-S445, 2013, doi: 10.1016/j.surfcoat.2012.05.033

[28] S. Kumar, T.S.N. Sankara, S. Sundara, *Thermal oxidation of CP Ti: an electrochemical and structural characterization,* Materials Characterization, vol. 61, iss. 6, pp. 589-597, 2010, doi: 10.1016/j.matchar.2010.03.002